Lab on a Chip

PAPER

View Article Online
View Journal | View Issue

Cite this: *Lab Chip*, 2016, **16**, 2126

High-throughput electrical measurement and microfluidic sorting of semiconductor nanowires†

Cevat Akin,[a] Leonard C. Feldman,[b] Corentin Durand,‡[c] Saban M. Hus,[c] An-Ping Li,[c] Ho Yee Hui,[d] Michael A. Filler,[d] Jingang Yi[a] and Jerry W. Shan*[ab]

Received 16th February 2016,
Accepted 4th May 2016

DOI: 10.1039/c6lc00217j

www.rsc.org/loc

Existing nanowire electrical characterization tools not only are expensive and require sophisticated facilities, but are far too slow to enable statistical characterization of highly variable samples. They are also generally not compatible with further sorting and processing of nanowires. Here, we demonstrate a high-throughput, solution-based electro-orientation-spectroscopy (EOS) method, which is capable of automated electrical characterization of individual nanowires by direct optical visualization of their alignment behavior under spatially uniform electric fields of different frequencies. We demonstrate that EOS can quantitatively characterize the electrical conductivities of nanowires over a 6-order-of-magnitude range (10^{-5} to 10 S m^{-1}, corresponding to typical carrier densities of 10^{10}–10^{16} cm^{-3}), with different fluids used to suspend the nanowires. By implementing EOS in a simple microfluidic device, continuous electrical characterization is achieved, and the sorting of nanowires is demonstrated as a proof-of-concept. With measurement speeds two orders of magnitude faster than direct-contact methods, the automated EOS instrument enables for the first time the statistical characterization of highly variable 1D nanomaterials.

Introduction

Over the past two decades, a tremendous variety of 1D nanomaterials with fascinating physical properties have been synthesized and explored as new building blocks in nanoelectronics,[1,2] photonics,[3,4] and energy conversion and storage,[5,6] among other applications.[7,8] Despite the importance of electrical conductivity for controlling many basic device functions, it is typically poorly known and can be highly variable even within a given sample. Surface functionalization, size effects, growth conditions, and intrinsic variations due to small numbers of charge carriers can all play important roles in determining the electrical-transport properties of individual nanowires.[9–11] To understand and control the functional variations of nanowires, and ultimately enable their use in nanodevices, it is necessary to develop high-throughput techniques to measure the conductivity of large numbers of individual nanowires. In addition to characterization, the accurate sorting and manipulation/assembly[12,13] of these materials are also highly desirable for building functional nanodevices.

Traditional, direct-contact methods using nanoprobes under SEM[14] or microfabricated electrodes,[15] can provide highly accurate measurements on small numbers of nanowires,[10] but typically take days for a few measurements and require specialized facilities. Other techniques such as atom probe tomography,[16] scanning photocurrent microscopy,[17] Kelvin probe force microscopy,[18] and electron holography[19] can spatially assess dopant distribution and carrier density, but are even more laborious and time-consuming. Because of their slow speed, existing direct-contact electrical characterization methods are poorly suited for the large number of measurements needed to statistically characterize highly variable samples.

We have recently demonstrated a new contactless, solution-based electro-orientation spectroscopy (EOS) method to efficiently measure the electrical conductivity of individual nanowires over a 5-order-of-magnitude range (10^{-5} to 1 S m^{-1}).[20] The EOS method is similar in spirit to the electric-field-based methods that have been developed for characterizing cells and viruses, including dielectrophoresis,[21] electro-rotation,[22]

[a] *Department of Mechanical and Aerospace Engineering, Rutgers University, Piscataway, NJ, 08854, USA. E-mail: jshan@jove.rutgers.edu*
[b] *Institute of Advanced Materials, Devices, and Nanotechnology, Rutgers University, Piscataway, NJ, 08854, USA*
[c] *Center for Nanophase Materials Sciences, Oak Ridge National Laboratory, Oak Ridge, TN, 37831, USA*
[d] *School of Chemical & Biomolecular Engineering, Georgia Institute of Technology, Atlanta, GA, 30332, USA*

† Electronic supplementary information (ESI) available: Direct-contact STM measurement of the *I–V* curves with different probe spacings, aspect-ratio measurements of as-produced and passivated Si nanowires by SEM, alignment of two individual Si nanowires at different frequencies under slow-rates and demonstration of sorting according to their electrical conductivities. See DOI: 10.1039/c6lc00217j

‡ Current address: Centre d'Elaboration des Matériaux et d'Etudes Structurales, B.P. 94347, 29 rue Jeanne Marvig, Toulouse, F-31055, France.

isodielectric separation,[23] and impedance spectroscopy.[24] However, previous attempts to extend these contactless methods to study the electrical properties of nanowires and nanotubes have been qualitative characterizations over a large population of 1D nanomaterials,[25,26] or have not been validated against other methods.[27] The EOS method, being quantitative and efficient, offers the unique potential to characterize and understand the fundamental statistical variability of 1D electronic materials.

Here, we extend the EOS method by automating it for high-throughput (relative to direct-contact methods) electrical characterization of 1D nanomaterials. We also increase the maximum measurable conductivity by an order of magnitude, and integrate the technique into a simple microfluidic device. The continuous-flow microfluidic device not only enables rapid characterization, but also, for the first time, sorting of nanowires by their measured conductivity. Automation allows the characterization of individual nanowires in less than a minute, which is two-orders of magnitude faster than traditional electrical-characterization techniques, and an order of magnitude faster than our previous implementation of EOS. Being solution-based, the EOS method is also compatible with other solution-based sorting and manipulation techniques for post-growth assembly of nanowire-based devices.

Briefly, in the case of electro-orientation, a freely suspended nanowire or nanotube rotates into alignment along the electric-field direction due to an induced dipole in the particle.[28,29] The particle motion can be analyzed by treating the nanoparticle as a polarizable lossy dielectric with homogeneous electrical properties immersed in a viscous fluid.[30–32] The alignment rate at different frequencies is a strong function (through the Clausius–Mossotti factor) of electrical properties of the particle and the frequency of the applied field. In particular, the alignment rate at low frequencies depends on the difference between the electrical conductivities of the particle and the suspending fluid, while the alignment rate at higher frequencies depends on the permittivities. The transition frequency between these two regimes, the crossover frequency, is found as the inverse of the Maxwell–Wagner time scale, $\tau_{MW,\|}$, *i.e.*,

$$\omega_{MW} = \frac{1}{\tau_{MW,\|}} = \frac{(1-L_\|)\sigma_f + \sigma_p L_\|}{(1-L_\|)\varepsilon_f + \varepsilon_p L_\|}, \quad (1)$$

where σ is the conductivity, ε is the permittivity, $L_\| \simeq \frac{1}{\beta^2}[\ln 2\beta - 1]$, is the geometric depolarization factor, β is the aspect ratio of the 1D nanoparticle and the subscripts f and p refer to the fluid and particle, respectively. In the simultaneous limit of high-aspect-ratio 1D nanomaterials, in which case the depolarization factor becomes very small (*e.g.*, $L_\| \lesssim 10^{-3}$ for $\beta \gtrsim 50$) and a very low-conductivity solvent, the crossover frequency further simplifies to depend only on the particle conductivity and fluid permittivity, and not on the (also unknown) particle permittivity:

$$\omega_{MW} \cong \frac{\sigma_p}{\varepsilon_f (L_\|^{-1} - 1)}. \quad (2)$$

In this case, the electrical conductivity of nanowires can be extracted using eqn (2) by measuring the alignment rates of the nanowires at different electric-field frequencies in a fluid of known permittivity. It should be noted that the simplified form of eqn (2), which assumes $(L_\|^{-1} - 1)\sigma_f \ll \sigma_p$, effectively requires that the fluid be much less conductive than the particle, *i.e.*, $\sigma_f/\sigma_p \ll L_\|$, for large-aspect ratio particles. If this requirement is not met, then eqn (1) should be used instead.

Results

We have automated the EOS technique with an algorithm implemented in LabVIEW (National Instruments Corp.) to rapidly and continuously characterize 1D nanomaterials, as schematically shown in Fig. 1. Electrodes were patterned *via* photolithography on a glass microscope slide to provide nearly spatially uniform electric-field in horizontal and vertical directions (see Methods for details). Alignment rate measurements were only taken in the central region of the electrode gap (200 × 100 μm) where the electric-field variation is less than than 10%. The microfluidic chip was placed on an inverted optical microscope (Olympus IX71, Olympus Corp.) with 40× objective lens accompanied with a high-speed monochrome CCD camera (pco.edge sCMOS, PCO AG) for direct optical visualization of the frequency-dependent nanowire alignment rates. AC electric fields of different frequencies were applied to the sample by an arbitrary waveform generator (AFG3022C, Tektronix Inc.) connected to a high-frequency amplifier (Trek 2100 HF, Trek Inc.). LabVIEW was used to actuate the electronic components of the system, and for real-time image acquisition and analysis, as shown in the flow chart in Fig. 1b. After image analysis to measure alignment rates as a function of frequency, the LabVIEW code finds the crossover frequency by fitting a curve to the data in the form of $\Omega = 1/[1 + (\omega/\omega_{MW})^2]$ where Ω is the normalized alignment rate and ω is the frequency of the applied electric field. The analysis algorithm then uses the fitted crossover frequency, ω_{MW}, to determine electrical conductivity using eqn (2). The effect of Brownian motion on the alignment-rate measurements and the computed conductivity is minimal, as discussed in the ESI.†

To demonstrate the technique, silicon nanowires (diameter: 50–300 nm, length: 5–30 μm) were fabricated using metal-assisted chemical etching (MACE) of doped Si wafers,[33] and nominally undoped germanium nanowires (diameter: 70–80 nm, length: 6–7 μm) were grown by the vapor–liquid–solid (VLS) technique[34] (see Methods for details). Silicon nanowires were characterized either as-produced (after annealing in vacuum) or with dry-oxygen passivation at 950 °C, while Ge nanowires were studied as produced. Nanowires were dispersed in either mineral oil or dipropylene glycol

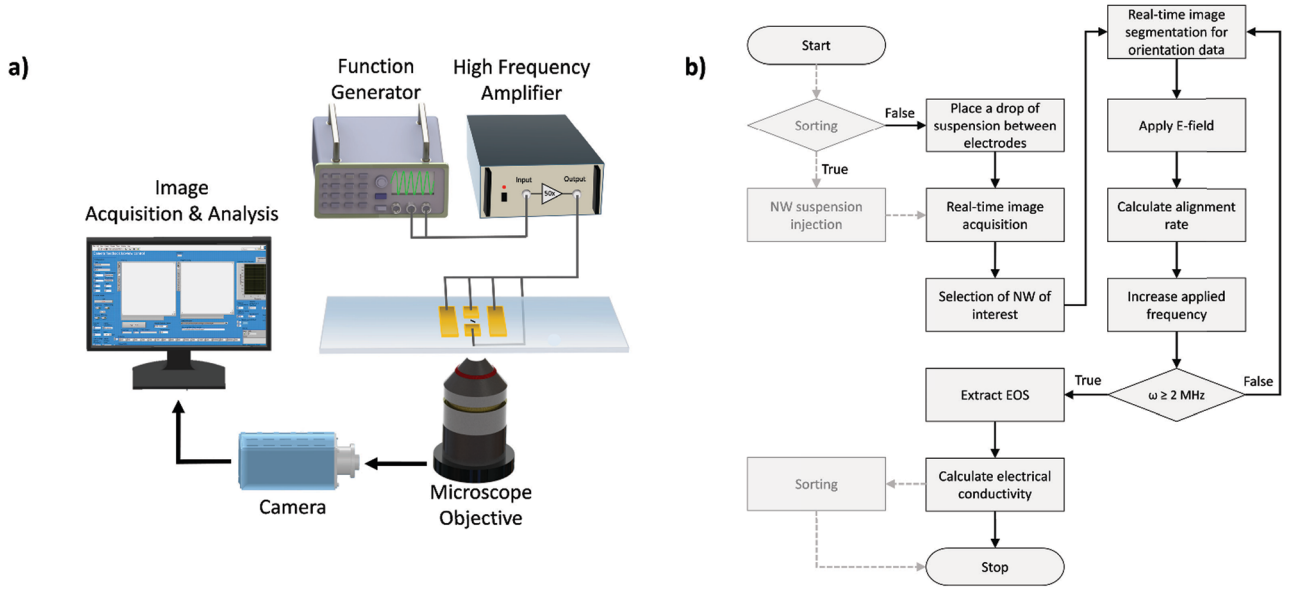

Fig. 1 Experimental schematic and block diagram of automation algorithm. a) Experimental setup to measure the alignment rates of the nanowires at different frequencies. A pair of axial electrodes apply uniform electric fields of different frequencies to align the nanowires, while a pair of cross-channel electrodes reorient the nanowires for repeated measurements at different frequencies. b) Flow chart of the electrical-conductivity-characterization algorithm, including image acquisition and analysis, control of the electronics and calculation of electrical conductivity. Dashed boxes show the optional sorting function.

(DPG). Both fluids have low electrical conductivity, which yields a thick double layer around the particles and minimizes induced-charge electro-osmotic flow at the particle–fluid interface.[35–37] The low conductivity of the solvent also enables the simplification of crossover frequency in eqn (1). Dipropylene glycol has a higher dielectric constant than mineral oil ($\varepsilon_{DPG}/\varepsilon_0 = 21$ *vs.* $\varepsilon_{oil}/\varepsilon_0 = 2.0$), giving it the potential to increase the measurement range to higher-conductivity particles by decreasing the crossover frequency.[35,37]

First, we demonstrated the repeatability of the automated EOS method in determining electrical conductivity by measuring an individual Si nanowire several times. Ten separate electro-orientation spectra were measured for the same nanowire. As seen in Fig. 2a, the measured alignment rates at different frequencies for an individual Si nanowire show the expected crossover behavior. The electro-orientation spectra also show excellent repeatability for the same nanowire, as indicated by the small error bars in Fig. 2a. For repeated measurements of the same nanowire, the fitted crossover frequency has a standard deviation that is 10% of the mean crossover.

Automation of the electrical conductivity determination enables the rapid characterization of many individual nanowires to obtain statistical information about the nanowire ensemble. To show this capability, we measured the electrical conductivities of 100 as-produced Si nanowires fabricated at the same time from a portion of one Si wafer.[33] The distribution of measured conductivities of this set of nanowires is broad, as shown in Fig. 2b, with a peak at 0.06 S m^{-1}. For comparison, we measured two nanowires from the same Si wafer using two-probe scanning tunneling microscopy (STM). The arrows in Fig. 2b show that the STM-measured conductivity values also have significant variability, which is consistent with the conductivity distribution measured by EOS (see Methods for detailed information about direct-contact STM measurements).[14,20]

Although there is good agreement between the EOS and direct-contact STM measurements, the measured conductivities were two orders of magnitude lower than the bulk conductivity of the original Si wafer ($2–3.3 \times 10^1\ \Omega^{-1}\ m^{-1}$). Therefore, we next investigated the importance of surface effects on the same n-type Si nanowires using dry-oxygen surface passivation.[20] We characterized 100 passivated Si nanowires *via* automated EOS and compared the results with STM-transport measurements, as seen in Fig. 2b. There was again good agreement between EOS and STM measurements, with both methods showing an order of magnitude increase in measured electrical conductivities after surface passivation. The higher conductivity of the passivated Si nanowires is due to the elimination of surface dangling bonds, which otherwise trap charge carriers in the nanowires. However, with the automated EOS using mineral oil as the solvent, ten out of the 100 measured Si nanowires had conductivities higher than could be measured ($\sigma_{EOS} \gg 1.2\ \Omega^{-1}\ m^{-1}$). This was because, for these nanowires, their crossover frequencies exceeded the bandwidth of the amplifier used to drive the electro-orientation.

To increase the measurement range, we next changed the suspending fluid to DPG, which has an order of magnitude higher permittivity than mineral oil (Table 1). As seen from eqn (1), the crossover frequency is expected to decrease by an order of magnitude, thus increasing the measurable

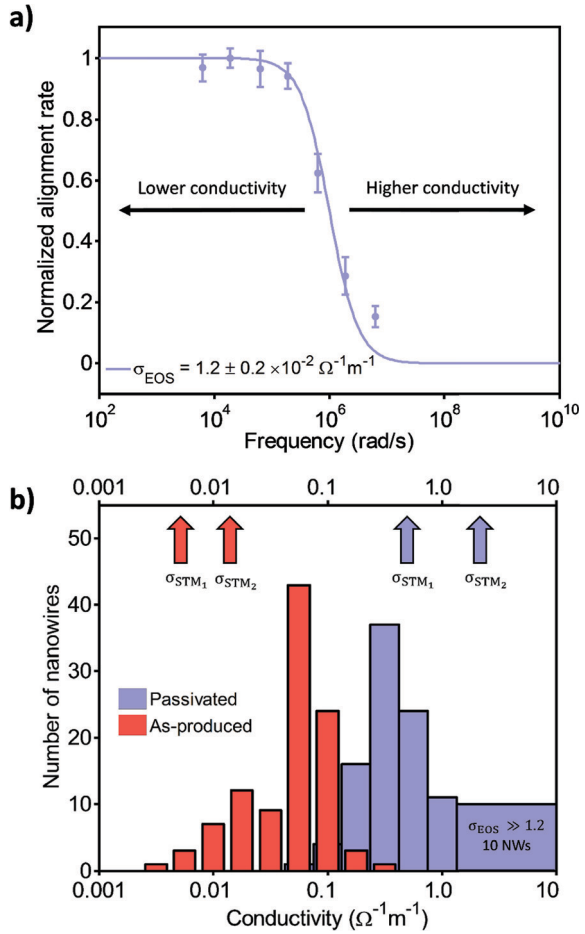

Fig. 2 Electro-orientation spectra and measured conductivity distributions for Si nanowires. a) Measured alignment rates of an individual as-produced Si nanowire with respect to applied electric-field frequency. Ten repeated measurements of the same nanowire show small variation between nanowires, as seen in the error bars. b) Measured conductivity distribution of 100 as-produced and 100 passivated Si nanowires. Arrows show the electrical conductivities of four individual nanowires measured *via* direct 2P-STM for comparison. Automation of the EOS technique enables two-orders-of-magnitude faster characterization than previously possible, with a measurement in less than one minute.[20]

conductivity for a fixed measurement-system bandwidth.[20] First, we dispersed as-produced Si nanowires in DPG and compared the electro-orientation spectra (Fig. 3a) with those measured using mineral oil as the solvent. A second crossover frequency (this time an increase in alignment rate) is seen in the low-frequency range (10^3–10^4 rad per s) when DPG is used as the suspending fluid. To understand the additional crossover frequency at the low frequencies, we considered the electrical double layer that forms on the particle/fluid interface due to accumulation of charges under the external electric field. The electrical double layer is expected to have a characteristic charging timescale, τ that scales inversely as the square-root of the fluid conductivity.[32,37] For electric-field frequencies below $f^* \equiv 1/\tau \propto \sqrt{\sigma_f}$, charging of the electrical double layer can significantly screen the applied field acting on the particle. Conversely, at frequencies much greater than f^*, the electric field at the particle is minimally affected by the electrical double layer in DPG, and the expected Maxwell–Wagner crossover behavior can be observed and used to determine the electrical conductivity. For mineral oil, which has an electrical conductivity 3 orders of magnitude lower than DPG (Table 1), the double layer is extremely thick and the charging timescale is longer than that of the lowest frequency used, so the low-frequency crossover is not seen.

To test the hypothesis that charging of the electrical double layer in the solvent is responsible for the low-frequency crossover in the alignment rate, we increased the electrical conductivity of DPG by 10× by adding 0.2 g l^{-1} of an ammonium salt, tetrabutylammonium tetraphenylborate. By addition of this salt, the observed low-frequency crossover is increased by 2.5–3 times, (Fig. 3a), consistent with the expected $\sqrt{10}$ increase in the f^* crossover due to double-layer charging. Critically, the addition of salt does not change the observed higher-frequency (Maxwell–Wagner) crossover that is used to measure the nanowire conductivity. Thus, changing the suspending fluid to a solvent of different electrical conductivity does not affect the measurement. Furthermore, we were able to obtain a one-order-of-magnitude decrease in the measured Maxwell–Wagner crossover frequency by switching to DPG from mineral oil. This allowed us to measure nanowires that have conductivities up to 10 S m^{-1}, which is an order-of-magnitude increase over our previous measurement range.[20] As seen in Fig. 3b and Table 1, using mineral oil,

Table 1 Statistics of the measured electrical conductivities of different nanowire samples and electrical properties of the suspending fluids

Nanowire type	Suspending fluid	Electrical properties of suspending fluid	Measured electrical conductivity statistics (Ω^{-1} m^{-1})
As-produced Si	Mineral oil	$\varepsilon_f/\varepsilon_0$ = 2.0 σ_f = 1.0 × 10^{-10} Ω^{-1} m^{-1}	Mean: 5.9 ± 0.7 × 10^{-2} Std: 3.9 × 10^{-2}
As-produced Si	DPG	$\varepsilon_f/\varepsilon_0$ = 21 σ_f = 1.0 × 10^{-7} Ω^{-1} m^{-1}	Mean: 6.0 ± 0.8 × 10^{-2} Std: 4.3 × 10^{-2}
As-produced Si	DPG + salt	$\varepsilon_f/\varepsilon_0$ = 21 σ_f = 1.0 × 10^{-6} Ω^{-1} m^{-1}	Mean: 6.3 ± 1.0 × 10^{-2} Std: 5.1 × 10^{-2}
Passivated Si	Mineral oil	$\varepsilon_f/\varepsilon_0$ = 2.0 σ_f = 1.0 × 10^{-10} Ω^{-1} m^{-1}	Mean: 4.3 ± 0.5 × 10^{-1} Std: 2.4 × 10^{-1}
As-produced Ge	DPG	$\varepsilon_f/\varepsilon_0$ = 21 σ_f = 1.0 × 10^{-7} Ω^{-1} m^{-1}	Mean: 8.2 ± 0.6 × 10^{0} Std: 2.9 × 10^{0}

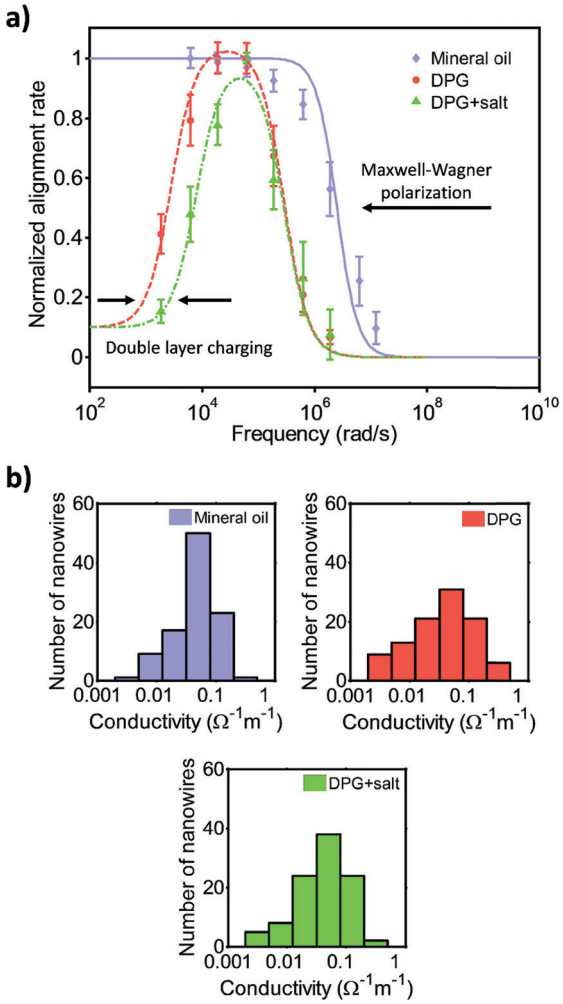

Fig. 3 Measured electro-orientation spectra and conductivities distributions for as-produced Si nanowires in different suspending fluids. a) Electro-orientation spectra of as-produced Si nanowires in different media showing traditional Maxwell–Wagner crossover frequency behavior as well as an additional, low-frequency crossover due to double-layer charging in the higher-conductivity DPG solution. b) Histograms of the measured electrical conductivities of 100 as-produced Si nanowires each in three different solvents show similar behavior.

DPG, and DPG + salt all give similar distributions, means, and standard deviations for as-produced Si nanowires. Thus, changing the suspending fluid to the higher-permittivity fluid like DPG, while increasing the measurement range of EOS to more conductive nanowires, does not affect its quantitative accuracy.

Nanowire ensembles can exhibit large diameter and length variations. Our dependence on diffraction-limited optical microscopy to visualize the nanowires can therefore introduce errors in the EOS measurements *via* uncertainties in the particle aspect ratio, which enters eqn (2) through the depolarization factor $L_{\|}$. While this increases the uncertainty for an individual measurement, it is nonetheless possible to accurately find the conductivity statistics of a sample using linear error analysis and the independently determined aspect-ratio distribution of the nanowire sample (*e.g.*, using SEM, TEM, or other means). Here, we demonstrate this procedure which was proposed but not implemented in an earlier paper.[20] We measured the aspect-ratio statistics of as-produced and passivated Si nanowires under SEM (ESI,† aspect-ratio measurements) and used linear error analysis to find the corrected conductivity statistics, as seen in Table 2. The mean conductivities increased somewhat, but the standard deviation of the measured conductivities remained large, at 37–54% of the mean. Thus, after correcting for size variations in the nanowires, the EOS measurements still show large variations in the conductivity of the Si nanowires. Variations in growth conditions, and surface and size effects, may all contribute to these within-ensemble conductivity variations, which are also seen in the STM measurements.

The increased measurement range enabled by DPG allows us to characterize higher-electrical-conductivity nanowires. To this end, the electrical conductivity of 37 as-produced, nominally undoped Ge nanowires was measured *via* EOS, as seen in Fig. 4. The measured electrical conductivity of the Ge nanowires was higher than the Si nanowires, and also higher than the previous measurement limit of $\sigma_{EOS,max} \leq 1.2\ \Omega^{-1}\ m^{-1}$. For comparison, the electrical conductivity of two Ge nanowires from the same sample was also measured *via* four-probe STM, as shown by the arrows in Fig. 4 (ESI,† *I–V* curves). The good agreement between the EOS and STM conductivity measurements further validates the accuracy of our method. It can be seen from Table 1 that the variation in the Ge nanowires is less than that between MACE-grown Si nanowires (all from the same sample), suggesting that the VLS technique as implemented here offers better structural uniformity and lower contamination, both of which affect the electrical conductivity.

Finally, being a solution-based technique, EOS can be implemented in a microfluidic device to continuously characterize the electrical conductivity of nanowires, and is compatible with other solution-based (*e.g.*, flow or electric-field manipulation) techniques to sort or assemble nanowires. To demonstrate this, we have build the simple microfluidic device shown in Fig. 5a. A digital craft cutter (Silhouette Portrait, Silhouette America Inc.) was used to cut a 500 μm wide channels on 50 μm thick pressure-sensitive double-sided tape (FLEXmount 100 clear, FLEXcon).[38] The tape was aligned on top of Cr/Au electrodes that were lithographically patterned and sputtered on a glass slide. The flow channel was then formed by adding an optically transparent, chemical-resistant

Table 2 Measured aspect-ratios and conductivity statistics of as-produced and passivated Si nanowires, before and after correction using linear error analysis[20]

Nanowire type	Aspect-ratio statistics	Measured electrical-conductivity statistics (Ω^{-1} m^{-1})	Corrected electrical-conductivity statistics (Ω^{-1} m^{-1})
As-produced	Mean: 77.0 Std: 28.8	Mean: 5.9×10^{-2} Std: 3.9×10^{-2}	Mean: 6.3×10^{-2} Std: 3.4×10^{-2}
Passivated	Mean: 136 Std: 51.5	Mean: 4.3×10^{-1} Std: 2.4×10^{-1}	Mean: 6.8×10^{-1} Std: 2.5×10^{-1}

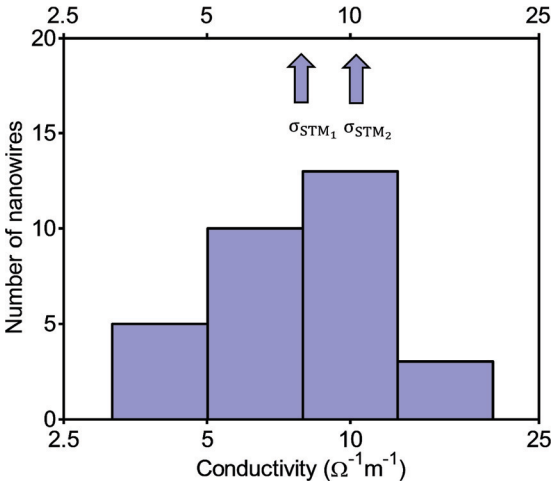

Fig. 4 EOS-measured conductivity distribution of VLS-grown Ge nanowires. Electrical conductivity of 37 Ge nanowires suspended in DPG were measured *via* EOS, taking advantage of the increased measurement range enabled by the higher-permittivity DPG. Arrows show the electrical conductivities measured by direct-contact STM probing that further validate the contactless EOS measurements.

PVC cover (#87545K121, McMaster-Carr), which had the necessary connections for driving the flow with syringe pumps (Pump 11 Pico Plus Elite, Harvard Apparatus). Flow focusing was used to concentrate the dilute nanowire suspension between the electrodes in the middle of the channel. Three pinch valves (#100P2NO-01S, Bio-Chem Fluidics) were connected to the tubing at the outlets to sort nanowires according to their electrical conductivities. The two valves controlling the outside outlet channels are normally closed, while the valve on the central outlet channel is normally open. Nanowires that are not characterized and sorted are directed to the normally open center channel. If a nanowire of the desired conductivity is identified by the automated EOS process, then it can be sorted to one of the side channels.

We first tested the microfluidic device without sorting ability (with a single inlet and outlet channel) to ensure that electrical characterization can remains accurate under flow in a microchannel. We measured the electrical conductivity of 100 as-produced Si nanowires in the microfluidic device, and compared to the distribution previously measured for as-

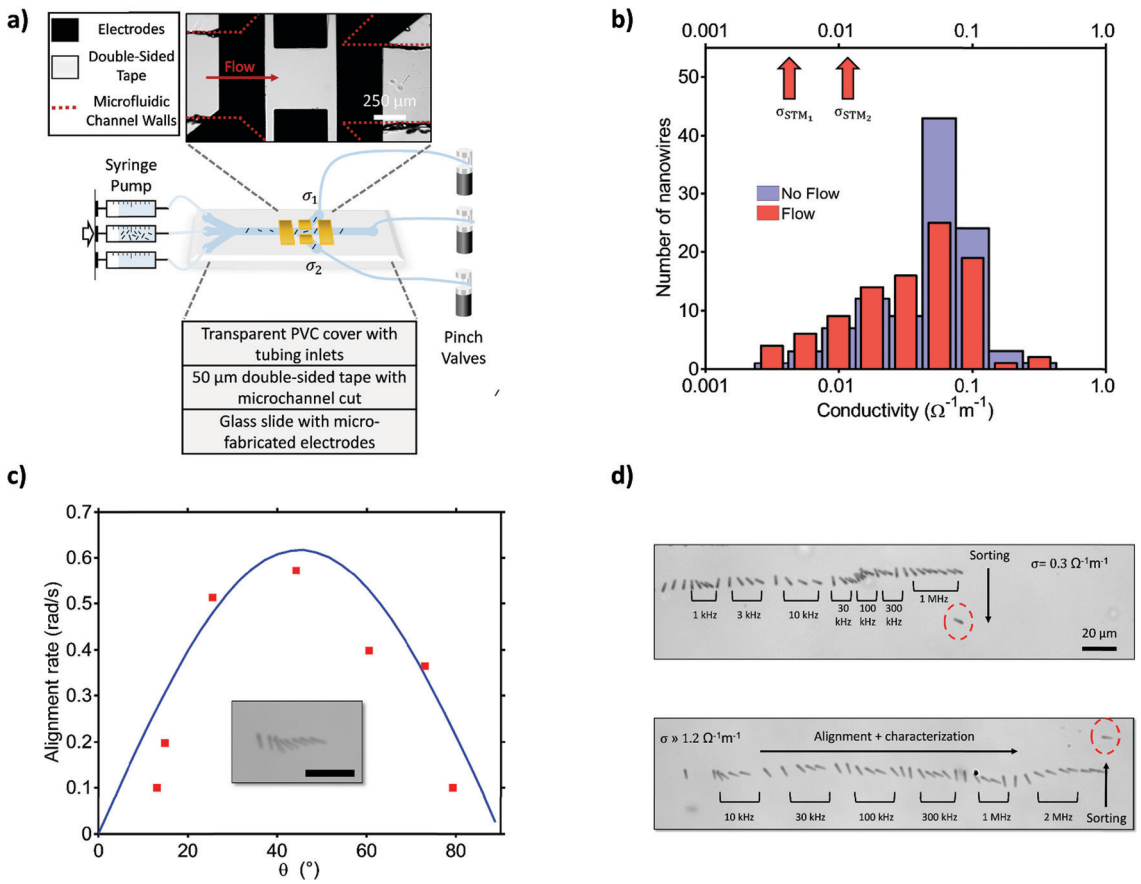

Fig. 5 Demonstration of microfluidic device for continuous-flow characterization and sorting of nanowires. a) A simple microfluidic channel, fabricated by cutting pressure-sensitive double-sided tape *via* craft-cutter, is aligned on top of microfabricated electrodes and covered with a transparent PVC cover that includes tubing connections for fluid injection. Pinch valves are used in the outlet channels to create positive pressure difference for sorting. b) Comparison of measured conductivity distributions for as-produced Si nanowires with and without flow where the flow rate was 5–10 nl min^{-1} for the flow case. c) Detail of measured alignment rate of Si nanowire under flow at 10 kHz as a function of nanowire angle with electric field. Inset: Overlay of images showing time series of nanowire alignment with horizontal electrical field, with scale bar corresponding to 20 µm. d) Sequence showing alignment of two different nanowires at different electric-field frequencies under flow, and sorting to different outlet channels according to measured electrical conductivities.

produced Si nanowires (Fig. 2b). There is good agreement in the distributions measured with and without flow, as seen in Fig. 5b. Furthermore, a detailed sequence showing alignment of a nanowire in the microchannel is shown in Fig. 5c at a single frequency, 10 kHz. There is good agreement between the theoretically expected and measured alignment rates as a function of nanowire angle relative to the electric field. Using data at different frequencies, we did not detect any significant differences in the measured electrical conductivities when the flow rates were in the range of 5–10 nl min^{-1}. Slow flow rates are necessary to avoid shear-induced alignment of the nanowires, and for the nanowire to have enough time in between the electrodes for EOS to determine the electrical conductivity of nanowires.

We then sorted nanowires according to their electrical conductivities by using pinch valves to create positive pressure differences that directed nanowires to different outlets. Fig. 5d shows the electrical characterization of two individual Si nanowires by the EOS method, followed by hydrodynamic sorting of these two individual nanowires into separate channels (ESI,† alignment/sorting video). Nanowires are first aligned with a horizontal field at a particular frequency, reset with a vertical field, and then horizontally aligned again at a different electric-field frequency. This process is repeated for each nanowire while they are flowing to measure the electro-orientation spectrum and determine the conductivity. For the two cases shown in Fig. 5d, one nanowire is measured to have a lower conductivity (σ_p = 0.3 Ω^{-1} m^{-1}) and is directed to the lower outlet, while another particle with a higher conductivity (σ_p = 1.2 Ω^{-1} m^{-1}) is directed to the upper outlet. Here, the sorting was done with pinch valves, but sorting of nanowires after characterization can also be achieved by means of electric-field manipulation techniques such as dielectrophoresis.[23,39]

Conclusions

Automation of the solution-based, contactless EOS technique allows for efficient quantitative electrical characterization of 1D nanomaterials. We have demonstrated the quantitative measurement of electrical conductivities of individual Si and Ge nanowires in less than a minute. This allows an effective rate (including sample preparation and loading) of hundreds of nanowires per day, which is at least two orders of magnitude faster than traditional direct-contact conductivity measurement using STM or microfabricated electrodes, and allows for the first time the statistical characterization of highly variable nanowires. The measurement range of EOS is also extended to 10× more conductive nanowires by changing low-permittivity mineral oil to higher-permittivity DPG. Using these two fluids, the measurement range of EOS is now six orders of magnitude, from 10^{-5} to 10 S m^{-1}. We showed that changing the suspending fluid does not affect the EOS measurement, although a new low-frequency crossover behavior is observed due to double-layer charging. Comparison between EOS and direct STM measurements show good agreement for both Si and Ge nanowires in both mineral oil and DPG. The EOS method has been incorporated into a simple microfluidic device to demonstrate the ability to continuously characterize and sort nanowires. Future designs could yield further improvements in both measurement range and speed, perhaps ultimately approaching the speed of modern cell-sorting techniques.[40] It is our hope that this technique will be a useful tool to better understand and control the functional variations of nanowires, and ultimately aid in their use in nanodevices.

Methods

Nanowire fabrication

Silicon nanowires were synthesized by a metal-assisted chemical-etching method described in detail elsewhere.[33] Briefly, a n-type Si wafer (2.0–3.3 × 10^{-1} Ω^{-1} m^{-1}) was washed with ethanol, acetone and DI water for ten minutes in each solvent. The wafer was then immersed in H_2SO_4 (97%) and H_2O_2 (35%) in a volume ratio of 3 : 1 for 30 minutes at room temperature, and then etched with 5% HF aqueous solution for 3 minutes at room temperature. The Si wafer was next placed into a Ag-coating solution containing 4.8 M HF and 0.005 M $AgNO_3$, which was slowly stirred for 1 minute. After a uniform layer of Ag nanoparticles coated the Si wafer, the wafer was rinsed with DI water to remove the excess Ag^+ ions and then immersed in an etchant composed of 4.8 M HF and 0.2 M H_2O_2. After 3 hours of etching in the dark at room temperature, the wafer was repeatedly rinsed with DI water and then immersed in dilute HNO_3 (1 : 1 v/v) for 60 minutes to dissolve the Ag catalyst. The wafer was washed with 5% HF again for 1 minute to remove the oxide layer, and then cleaned with DI water and dried under N2 flow. As-produced Si nanowires were in some cases treated with dry-oxygen passivation (950 °C for 15 minutes) immediately before testing to reduce surface-state densities. Both as-produced and passivated Si nanowires were vacuum annealed at 350 °C for several hours prior to testing.

Epitaxial Ge nanowires were grown from Au nanoparticle catalyst seeds in a previously described cold-wall chemical-vapor-deposition reactor (FirstNano, Easy Tube 3000).[34] Single-side polished Ge(111) wafers (MTI Corporation, CZ, 42–64 Ω cm) were cleaned with 10% HF (J.T. Baker) before immersion into a suspension of citrate-stabilized 30 nm Au colloid (Ted Pella) containing 0.1 M HF for 5 min. Substrates are then rinsed with 10% HF and deionized water, dried with nitrogen, and placed inside the growth reactor. Nanowire growth occurred at 370 °C with germane (GeH_4, 99.999%, Matheson Tri-Gas), trimethylsilane (TMS, 99.99%, Voltaix), argon (Ar, 99.999%, Air Products) flow rates of 25, 7, and 617 sccm, respectively. The total reactor pressure was 7 Torr.

Electrode fabrication

Glass slides were washed with acetone, isopropanol and DI water for 10 minutes each, dried using filtered air, and baked in a 200 °C oven for 30 minutes to remove organic residues.

Approximately 3 μm of S1818 photoresist (Shipley Photoresist, MicroChem Corp) was spin coated onto the slides, baked at 120 °C for 4 minutes, and then patterned with a mask aligner (EVG 620, EVGroup) at 120 mJ cm^{-2}. The slides were immersed in MF-319, photoresist developer (MicroChem Corp.), for 1–4 minutes to dissolve the exposed features, allowing the remaining photoresist to act as a masking layer for metal deposition. Upon completion of developing, substrates were rinsed with DI water, dried with filtered air, and hard baked in an oven at 120 °C for 30 minutes. Following inspection, the substrates were etched in dilute HF for 1 minute and allowed to dry in 65 °C. The substrates were then placed in metal deposition chamber (PVD 75, Kurt J. Lesker Company) for Cr/Au sputtering, following 12 hours system pump down to allow a vacuum formation of less than 5×10^{-15} Torr. First chromium then gold was sputtered onto the substrates for a total of 16 minutes to create electrodes with an estimated 1 nm thickness. In the metal lift-off process, the substrates were placed in an acetone solution with gentle agitation to lift off the photoresist, leaving patterned electrodes in place. The substrates were finally washed with DI water, inspected and dried in an oven at 65 °C.

Transport measurements by STM

Transport measurements were carried out at room temperature with a four-probe STM (Unisoku/RHK, Unisoku Co., Ltd.) as described in detail elsewhere.[10] Briefly, a drop of nanowire/ethanol dispersion was placed on a SiO_2-coated Si substrate and then introduced into the UHV system (base pressure $<2 \times 10^{-10}$ Torr). The samples were first annealed at a temperature of 250–300 °C, and then transferred to the characterization platform containing four STM probes and an *in situ* SEM. Probes were made by electrochemically etching tungsten. Contacts between probes and nanowires were established with the guidance of the STM scanner and SEM image. The transport measurements were performed with a sourcemeter (Keithley 6430, Keithley Instruments Inc.). In the case of Si nanowires, comparisons between two-probe and four-probe measurements showed that the contact resistance of the probes was negligible, so measurements were conducted with only two probes. Four-probe were used for resistivity measurements on Ge nanowires due to their higher conductivity, which makes the contribution of contact resistances more important.

Acknowledgements

This work of CA and JWS was supported in part by the National Science Foundation (CBET 0644719) and by the Chemical and Biological Technologies Department of the Defense Threat Reduction Agency (DTRA-CB) *via* grant BA12PHM123 in the "Dynamic Multifunctional Materials for a Second Skin D[MS]2" program. HYH and MAF acknowledge the support of the National Science Foundation (CBET 1150755). Four-probe STM measurements (C. D., S. M. H., and A.-P. L.) were conducted at the Center for Nanophase Materials Sciences, which is sponsored at Oak Ridge National Laboratory by the Scientific User Facilities Division, Office of Basic Energy Sciences, U.S. Department of Energy.

References

1 W. Lu and C. M. Lieber, *Nat. Mater.*, 2007, **6**, 841–850.
2 Y. Cui, Z. Zhong, D. Wang, W. U. Wang and C. M. Lieber, *Nano Lett.*, 2003, **3**, 149–152.
3 J. Wang, M. S. Gudiksen, X. Duan, Y. Cui and C. M. Lieber, *Science*, 2001, **293**, 1455–1457.
4 R. Yan, D. Gargas and P. Yang, *Nat. Photonics*, 2009, **3**, 569–576.
5 M. Law, L. E. Greene, J. C. Johnson, R. Saykally and P. Yang, *Nat. Mater.*, 2005, **4**, 455–459.
6 H. Kim and J. Cho, *Nano Lett.*, 2008, **8**, 3688–3691.
7 F. Patolsky and C. M. Lieber, *Mater. Today*, 2005, **8**, 20–28.
8 Y. Cui, Q. Wei, H. Park and C. M. Lieber, *Science*, 2001, **293**, 1289–1292.
9 P. M. Koenraad and M. E. Flatté, *Nat. Mater.*, 2011, **10**, 91–100.
10 A.-P. Li, K. W. Clark, X.-G. Zhang and A. P. Baddorf, *Adv. Funct. Mater.*, 2013, **23**, 2509–2524.
11 E. Roduner, *Chem. Soc. Rev.*, 2006, **35**, 583–592.
12 K. Yu, J. Yi and J. Shan, *IEEE Trans. Autom. Sci. Eng.*, 2015, **12**, 37–49.
13 K. Yu, J. Yi and J. Shan, *2015 IEEE Inter. Conf. on Automat. Sci. Eng.*, 2015, pp. 489–494.
14 T.-H. Kim, Z. Wang, J. F. Wendelken, H. H. Weitering, W. Li and A.-P. Li, *Rev. Sci. Instrum.*, 2007, **78**, 123701.
15 W. Gu, H. Choi and K. K. Kim, *Appl. Phys. Lett.*, 2006, **89**, 253102.
16 D. E. Perea, J. E. Allen, S. J. May, B. W. Wessels, D. N. Seidman and L. J. Lauhon, *Nano Lett.*, 2006, **6**, 181–185.
17 J. E. Allen, D. E. Perea, E. R. Hemesath and L. J. Lauhon, *Adv. Mater.*, 2009, **21**, 3067–3072.
18 E. Koren, Y. Rosenwaks, J. Allen, E. Hemesath and L. Lauhon, *Appl. Phys. Lett.*, 2009, **95**, 092105.
19 M. McCartney, M. Gribelyuk, J. Li, P. Ronsheim, J. McMurray and D. J. Smith, *Appl. Phys. Lett.*, 2002, **80**, 3213–3215.
20 C. Akin, J. Yi, L. C. Feldman, C. Durand, S. M. Hus, A.-P. Li, M. A. Filler and J. W. Shan, *ACS Nano*, 2015, **9**, 5405–5412.
21 M. Castellarnau, A. Errachid, C. Madrid, A. Juarez and J. Samitier, *Biophys. J.*, 2006, **91**, 3937–3945.
22 J. Yang, Y. Huang, X. Wang, X.-B. Wang, F. F. Becker and P. R. Gascoyne, *Biophys. J.*, 1999, **76**, 3307–3314.
23 M. D. Vahey and J. Voldman, *Anal. Chem.*, 2009, **81**, 2446–2455.
24 T. Sun, D. Holmes, S. Gawad, N. G. Green and H. Morgan, *Lab Chip*, 2007, **7**, 1034–1040.
25 R. Krupke, F. Hennrich, H. V. Löhneysen and M. M. Kappes, *Science*, 2003, **301**, 344–347.
26 D. H. Shin, J.-E. Kim, H. C. Shim, J.-W. Song, J.-H. Yoon, J. Kim, S. Jeong, J. Kang, S. Baik and C.-S. Han, *Nano Lett.*, 2008, **8**, 4380–4385.

27 D. Fan, F. Q. Zhu, X. Xu, R. C. Cammarata and C. Chien, *Proc. Natl. Acad. Sci. U. S. A.*, 2012, **109**, 9309–9313.
28 T. B. Jones, *Electromechanics of Particles*, Cambridge University Press, 2005.
29 H. Morgan and N. G. Green, *AC Electrokinetics: Colloids and Nanoparticles*, Research Studies Press, 2003.
30 M. S. Brown, J. W. Shan, C. Lin and F. M. Zimmermann, *Appl. Phys. Lett.*, 2007, **90**, 203108.
31 F. M. Zimmermann and J. W. Shan, *Appl. Phys. Lett.*, 2009, **94**, 053107.
32 R. J. Castellano, C. Akin, G. Giraldo, S. Kim, F. Fornasiero and J. W. Shan, *J. Appl. Phys.*, 2015, **117**, 214306.
33 K. Peng, J. Hu, Y. Yan, Y. Wu, H. Fang, Y. Xu, S. Lee and J. Zhu, *Adv. Funct. Mater.*, 2006, **16**, 387–394.
34 I. R. Musin and M. A. Filler, *Nano Lett.*, 2012, **12**, 3363–3368.
35 J. J. Arcenegui, P. García-Sánchez, H. Morgan and A. Ramos, *Phys. Rev. E: Stat., Nonlinear, Soft Matter Phys.*, 2013, **88**, 063018.
36 K. A. Rose, J. A. Meier, G. M. Dougherty and J. G. Santiago, *Phys. Rev. E: Stat., Nonlinear, Soft Matter Phys.*, 2007, **75**, 011503.
37 T. M. Squires and M. Z. Bazant, *J. Fluid Mech.*, 2004, **509**, 217–252.
38 P. K. Yuen and V. N. Goral, *Lab Chip*, 2010, **10**, 384–387.
39 D. R. Gossett, W. M. Weaver, A. J. Mach, S. C. Hur, H. T. K. Tse, W. Lee, H. Amini and D. Di Carlo, *Anal. Bioanal. Chem.*, 2010, **397**, 3249–3267.
40 C. W. Shields IV, C. D. Reyes and G. P. López, *Lab Chip*, 2015, **15**, 1230–1249.

